

Beyond End-Effector: Utilizing High-Resolution Tactile Signals for Physical Human-robot Interaction

Yu Sun, Cong Xiao, Lipeng Chen, *Member, IEEE*, Lu Chen, Haojian Lu, *Member, IEEE*, Yue Wang, *Member, IEEE*, Wang-Wei Lee, *Member, IEEE*, Yu Zheng, *Senior Member, IEEE*, Zhengyou Zhang, *Fellow, IEEE*, Rong Xiong, *Senior Member, IEEE*

Abstract—his article proposes a control framework for robots to apply their entire body as potential effectors in physical human-robot interaction (pHRI) tasks. This article proposes a control framework for robots to apply their entire body as potential effectors in physical human-robot interaction (pHRI) tasks. This framework is implemented based on high-resolution electronic skin that covers the entire body of the robot. During pHRI, robots must respond appropriately to human intentions, necessitating advanced sensing capabilities to interpret tactile information effectively. However, both discerning human intention from such large-scale tactile data and accommodating interaction across the entire body's surface present challenges. In this paper, we propose a method to convert the large-area contact on a link into a contact center and estimate the corresponding wrench. Furthermore, we assign soft priorities and desired trajectories to each contact point and solve for the optimal joint velocities through quadratic programming (QP). By enabling a dual-arm mobile manipulator to dance the waltz with a human, our control framework has been validated for its effectiveness in handling multiple large-area contacts and time-varying pHRI tasks.

Index Terms—Physical human-robot interaction, Artificial robot skin, Admittance control, Quadratic programming.

I. INTRODUCTION

ESILY deployable electronic skins have brought exciting new possibilities for the robotics community. These skins are extensively attached to the body of robots and have been successfully integrated into robotic systems [1–4]. Unlike traditional force/torque (F/T) sensors, the remarkable superiority of robot skins lies in their ability to envelop the robot's entire body, providing feedback on external forces and contact positions from every taxel. This feature makes it possible for

This work was supported in part by the Zhejiang Provincial Natural Science Foundation of China (LD22E050007), in part by the National Natural Science Foundation of China (62303407), in part by the Key R&D Program of Zhejiang (2022C01022, 2023C01176), and in part by Tencent Robotics X. (Corresponding authors: Haojian Lu and Lipeng Chen.)

Yu Sun, Cong Xiao, Lu Chen, Haojian Lu, Yue Wang, and Rong Xiong are with the State Key Laboratory of Industrial Control Technology, Zhejiang University, Hangzhou, Zhejiang 310027, China (e-mail: sunyuu@zju.edu.cn; congx@zju.edu.cn; lu-chen@zju.edu.cn; luhaojian@zju.edu.cn; wangyue@iipc.zju.edu.cn; rxiong@zju.edu.cn).

Lipeng Chen, Wang-Wei Lee, Yu Zheng, and Zhengyou Zhang are with the Tencent Robotics X Laboratory, Shenzhen 518057, China (e-mail: lipengchen@tencent.com; wwlee@tencent.com; petezheng@tencent.com; zhengyou@tencent.com).

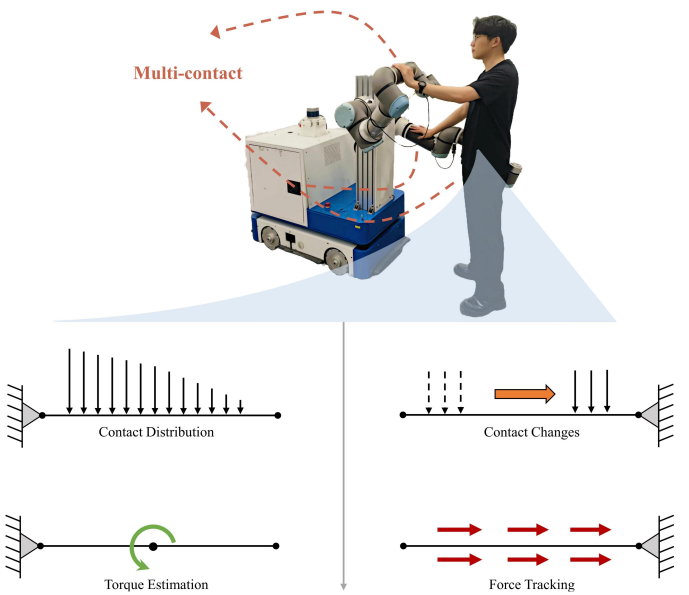


Fig. 1. Depiction of a waltz between a human and a robot. The distribution and alterations in contact can be interpreted as torque and track force applied at the contact center.

large-scale physical human-robot interaction (pHRI) virtually anywhere. In other words, *robot skin enables every part of the robot body to serve as a potential effector*.

In the realm of pHRI, the standard approach entails integrating a six-axis F/T sensor at the end-effector of the manipulator and employing impedance control (admittance control) [5, 6] in Cartesian space to react to external force. However, we have discovered that relying solely on interaction at the end-effector level is often inadequate for many pHRI tasks. This inadequacy arises not only due to the potential existence of multiple contact points but also because the interaction may need to encompass a considerable area. Such tasks could include moving large, unwieldy objects or engaging in more human-like activities, like waltzing between a human and a robot. As depicted in Fig. 1, during a waltz between a human and a robot, multiple contact areas emerge simultaneously between them. The human guides the robot's movements by adjusting the force and force distribution applied to the robot's links from his waist.

Recognizing human intention from tactile-based pHRI while

ensuring appropriate robot motion poses significant challenges. Unlike point-specific F/T sensors, this kind of robot skins need extensive contacts and thus can hardly directly perceive external torques. Additionally, many current tactile sensors are limited to detecting normal forces, neglecting shear forces [7]. For Cartesian admittance control, six-dimensional forces and torques are essential. Moreover, the robot's entire body comprises numerous potential contact locations, each representing an interaction task. The robot often lacks the necessary capability to perform all interaction tasks simultaneously. Considering the unpredictability of contact points, predetermining a desired trajectory for every individual point proves unfeasible.

Based on these observations, in this paper, we focus on tactile-based wholebody pHRI tasks. Unlike previous works [8] that mainly emphasize maintaining compliance, our work focuses on interpreting tactile signals within Cartesian space to enable complex, large-area physical interaction behaviors. To achieve this, we propose a comprehensive tactile signals processing framework. This framework is aimed at converting extensive contact information into Cartesian space, assigning tasks and corresponding priorities to each contact point. We have conducted extensive physical experiments to demonstrate the effectiveness of our proposed method. In summary, the detailed contributions of this paper are as follows:

- 1) We develop a method utilizing high-resolution tactile contact to identify the contact center and associated wrench. Unlike previous studies, our method discerns torque through contact distribution and generates estimated forces to track changes in contact to adapt to external experimental variations.
- 2) We introduce an automated method to generate the reference trajectories for individual contact centers and prioritize them within the task stack. This enables smooth robot motions amidst time-varying external contacts.
- 3) We determine the optimal joint velocity command while adhering to robot physical constraints. We validate our method through a series of experiments, including a human-robot dance scenario. To the best of our knowledge, it is the first experimental result of a complicated dance between a human and a robot using the distribution and variation of large-scale contact.

This paper is organized according to the following structure. Section II describes the related works of wholebody physical interaction and Section III introduces our system. Section IV introduces the determination of the contact center and corresponding wrench. In Section V, the desired trajectories and priorities for each contact center are set. Section VI discusses the experiments and obtained results. Finally, conclusions are drawn in Section VII.

II. RELATED WORKS

Numerous studies on pHRI often see contact information as a trigger signal or are tailored for specific robot types, which contrasts with our motivation. In the realm of wholebody pHRI, a common strategy involves projecting all contacts into joint space for unified processing. In scenarios lacking tactile

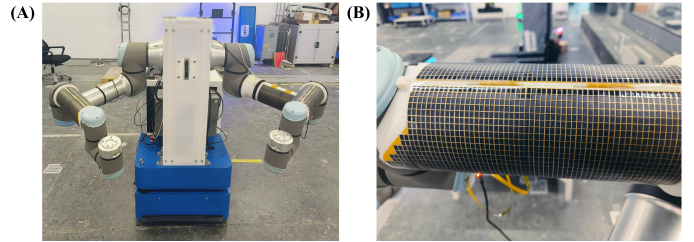


Fig. 2. Our Hardware Architecture. (A) A complete view of our dual mobile manipulator with tactile cover. (B) Detailed view of our high-resolution electronic skin.

sensors, these contacts can be identified through joint torque sensors [9, 10] or compliant mechanisms like elastic joints [11, 12]. Sadeghian et al. [13] introduced a controller-observer to estimate external contact, and employ joint space impedance control to respond to these contacts.

Electronic skin enables direct acquisition of contact information. Following calibration, detected forces can be transformed either to the center of mass [14] or into joint space using the principle of virtual work [15–18]. Leboutet et al. [19] proposed a hierarchical force propagation approach prioritizing the transfer of forces detected on robot skin to the upper limb's joint space. This method seamlessly integrates with tasks such as obstacle avoidance [18] and humanoid robot balancing [17]. Guadarrama et al. [20] introduced a concept of virtual torque based on contact distribution to enhance wrench information, consolidating forces in a patch and applying them uniformly in joint space. These transmission methods focus on maintaining compliance but may not fully exploit the robot's capabilities for active task execution.

Transforming each contact point into Cartesian coordinates establishes a direct correlation between applied forces and resulting motion. Although impedance control can be implemented without the need for F/T sensors, it is necessary to predefine the contact positions when modeling the control framework [21]. In the absence of tactile skin, sensors like RGB-D cameras [22] become essential for estimating contact positions and forces. Tactile sensors eliminate the need for these estimation processes. Leboutet et al. [8] adapted the zero moment point concept from legged robots, consolidating multiple contact forces into a force centroid and redirecting unresponsive upper limb forces to the base. The primary challenge with Cartesian space transmission method revolves around precisely identifying contact point locations, determining the wrenches exerted there, and then devising corresponding trajectories and priority schemes.

III. SYSTEM OVERVIEW

A. Hardware Architecture

Our hardware architecture is depicted in Fig. 2(A). Our robot platform is a dual-arm mobile manipulator, comprising an omnidirectional mecanum base and two UR16e manipulators with 6 degrees of freedom. Moreover, three electronic skins are integrated into the arms, two on the left arm and one on the right. Both the base and manipulators are velocity-controlled.

Displayed in Fig. 2(B), our electronic skin has exceptional resolution, with each taxel comprising a square measuring $0.0075m$ per side and interfacing with the main program at a frequency of $500Hz$. Each taxel is capable of furnishing feedback regarding the normal contact exerted upon it. Additionally, we chose the link's reference frame as defined by the D-H table, and described the position of the skin's taxel within this reference frame.

We calibrated our electronic skin, ensuring accuracy in both the normal force ${}^i\mathbf{f}_{\sigma_{ij}} \in \mathbb{R}^3$ measurements for each taxel and their position ${}^i\mathbf{p}_{\sigma_{ij}} \in \mathbb{R}^3$ relative to the link's reference frame O_{γ_i} . When the force detected on a taxel exceeds a predefined threshold $\sigma_t \in \mathbb{R}$, denoted as $\|{}^i\mathbf{f}_{\sigma_{ij}}\| > \sigma_t$, we identify this taxel as "in contact". This threshold is strategically set to mitigate zero-drift phenomenon. In our calibration process, we operate under the assumption that each taxel maintains a rigid attachment to the link, with fixed relative distances between them. Consequently, determining the precise position of each taxel in relation to the reference frame O_{γ_i} becomes straightforward based on the taxel's index, while the pose ${}^0\mathbf{R}_{\sigma_{ij}} \in \mathbb{R}^{3 \times 3}$ of each taxel can be effectively represented by the pose ${}^0\mathbf{R}_i \in \mathbb{R}^{3 \times 3}$ of the attached link. It is worth noting that we do not consider the stretchable materials.

B. Kinematic Solution with Soft Task Priority

Our system coordinates $\mathbf{q}^\top = [\mathbf{q}_b^\top \quad \mathbf{q}_a^\top] \in \mathbb{R}^n$ are comprised of the unconstrained degrees of freedom of the mobile platform, described as a reduced state $\mathbf{q}_b = [x \quad y \quad \theta_{yaw}]^\top \in \mathbb{R}^3$, and the joint coordinates of the arm $\mathbf{q}_a \in \mathbb{R}^{n_a}$. We can assume that the interaction task is mathematically represented by $\mathbf{x} \in \mathbb{R}^6$ in Cartesian space, which contains the translation and the rotation. The direct kinematics mapping is described by $\mathbf{x} = f(\mathbf{q})$. Upon performing differentiation of this equation, we obtain:

$$\dot{\mathbf{x}} = \mathbf{J}(\mathbf{q})\dot{\mathbf{q}} \quad (1)$$

where $\mathbf{J}(\mathbf{q}) = \partial f(\mathbf{q})/\partial \mathbf{q}$ is the $6 \times n$ task Jacobian matrix. When our manipulator exhibits redundancy concerning the designated task, it can be established that the inequality $6 < n$.

At a given state of the robot (\mathbf{q}), the joint velocity corresponding to a desired task velocity $\dot{\mathbf{x}}$ can be obtained as follows:

$$\dot{\mathbf{q}} = \mathbf{J}^\# \dot{\mathbf{x}} + \mathbf{P} \dot{\mathbf{q}}_0 \quad (2)$$

where $\mathbf{J}^\# \in \mathbb{R}^{n \times 6}$ is the pseudo-inverse of Jacobian matrix \mathbf{J} , $\dot{\mathbf{q}}_0 \in \mathbb{R}^n$ is an arbitrary joint velocity and $\mathbf{P} = \mathbf{I} - \mathbf{J}^\# \mathbf{J}$ is the nullspace projector of \mathbf{J} . This can also be interpreted as one of the solutions to the following problem:

$$\chi^* = \min_{\chi} \|\mathbf{A}\chi - \mathbf{b}\|^2 \quad (3)$$

where $\mathbf{b} = \dot{\mathbf{x}}$, $\mathbf{A} = \mathbf{J}$ and $\chi = \dot{\mathbf{q}}$. In this way, we can transform it into a QP problem.

Considering that robots typically face tasks with different priorities, researchers have proposed two priority strategies [23]: employing a soft priority approach for simultaneous execution and adopting a strict priority strategy for hierarchical execution. Because methods based on strict priority can cause abrupt changes in joint velocity when switching task priorities

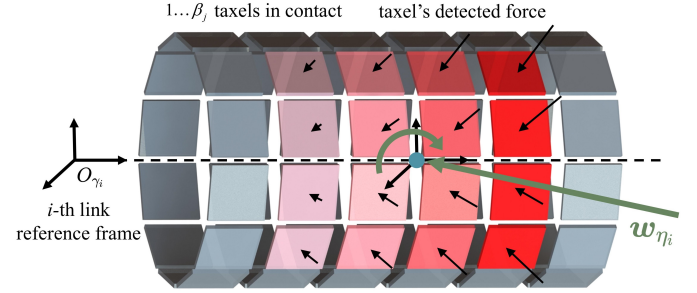


Fig. 3. Illustration of transforming large area contact of link i to contact center η_i . The darker the red color on the taxel, the greater the force applied to it.

[24], we primarily discuss methods based on soft priorities here.

Soft priority treats each task as the same level by setting a corresponding weight for each task, and executes them simultaneously. The allocation of weights is relative across tasks, with those possessing higher weights being accorded higher priority. Given a set of tasks with their relative weights ψ_i , the new QP problem becomes:

$$\chi^* = \min_{\chi} \sum_{i=1}^p \psi_i \|\mathbf{A}_i \chi - \mathbf{b}_i\|^2 \quad (4)$$

In Table I, the primary components utilized throughout this paper are presented. The superscript 0 and i means world frame and the link i 's reference frame, respectively.

IV. TACTILE-BASED PERCEPTION AND ESTIMATION

A. Large-area Contact Centering

As stated in Section III-B, achieving accurate control of tactile contact in Cartesian space necessitates condensing extensive contact area into a singular contact point. In the previous works, the force centroid method [8] struggled to accurately estimate the distribution of contact as torques, while methods centered around a fixed reference frame [20] failed to reflect the actual position of contact. To accurately represent the contact position while offering feedback on contact distribution, we opted for the geometric center derived from all taxels in contact as the designated contact center affixed to the link.

In specific case, we define the contact center of link i as O_{η_i} . Let's consider the scenario depicted in Fig. 3, where there are β_j taxels are in contact. By harnessing the data relayed by these taxels, we can acquire both the position ${}^i\mathbf{p}_{\sigma_{ij}}$ of these taxels relative to the reference frame of the attached link i . The position of contact center ${}^i\mathbf{p}_{\eta_i}$ can be regarded as the weighted mean of ${}^i\mathbf{p}_{\sigma_{ij}}$:

$${}^i\mathbf{p}_{\eta_i} = \frac{\sum_{j=1}^{\beta_j} \omega_{\sigma_{ij}} {}^i\mathbf{p}_{\sigma_{ij}}}{\sum_{j=1}^{\beta_j} \omega_{\sigma_{ij}}} \quad (5)$$

where $\omega_{\sigma_{ij}}$ is the weight of taxel σ_{ij} to adjust the force sensitivity across different positions on link i . Such sensitivity is a key feature of electronic skin, enabling us to determine the spatial variation in the importance of contact across the link i , which is an essential characteristic of the natural skin. The weight $\omega_{\sigma_{ij}}$ cannot be influenced by the detected force¹. Notably, given that each taxel's pose ${}^0R_{\sigma_{ij}}$ can be represented by the pose of its respective attached link 0R_i , we assert that the contact center shares the same pose as it is reference frame O_{γ_i} , i.e. ${}^0R_{\eta_i} = {}^0R_i$.

Another significant advantage of this approach is the elimination of the need to individually incorporate each taxel into the kinematic chain based on its position. There's no requirement to calculate the position of each taxel in world frame ${}^0x_{\sigma_{ij}}$ or derive its Jacobian matrix $J_{\sigma_{ij}}$. Considering the high resolution of our tactile sensor, this reduces our computational time significantly, sparing us from the tedious task of kinematic calibration for each taxel [25]. In this paper, we only need to compute the kinematics of the contact center in real-time. We can simply obtain the position of the contact center in world frame:

$${}^0p_{\eta_i} = {}^0R_i{}^i p_{\eta_i} + {}^0p_{\gamma_i} \quad (6)$$

Upon performing differentiation of this equation, we obtain²:

$${}^0\dot{p}_{\eta_i} = {}^0\dot{R}_i{}^i p_{\eta_i} + {}^0R_i{}^i \dot{p}_{\eta_i} + {}^0\dot{p}_{\gamma_i} \quad (7)$$

Referring to Eq. (1) and representing the differential of rotation matrix in a different way, we obtain:

$${}^0\dot{p}_{\eta_i} = [{}^0\omega_i]^\times {}^0R_i{}^i p_{\eta_i} + {}^0R_i{}^i \dot{p}_{\eta_i} + J_{p,\gamma_i} \dot{q} \quad (8)$$

In the above equation, $J_{p,\gamma_i} \in \mathbb{R}^{3 \times n}$ represents the position Jacobian matrix of the reference joint frame O_{γ_i} , ${}^0\omega_i \in \mathbb{R}^3$ is the angular velocity and $[{}^0\omega_i]^\times \in \mathbb{R}^{3 \times 3}$ is the skew-symmetric matrix of ${}^0\omega_i$. By doing so, we can describe the kinematics of the contact center η_i using the kinematics of reference frame γ_i .

We consolidate all detected forces ${}^0f_{\sigma_{ij}}$ into a resultant force ${}^0f_{\eta_i}$ and estimate the torque ${}^0\tau_{\eta_i}$ acting on the contact center. This is achieved by computing the cross-product of the force exerted by each taxel and the respective distance between each taxel and the contact center:

$${}^i f_{\eta_i} = \sum_{j=1}^{\beta_j} \omega_{\sigma_{ij}} {}^i f_{\sigma_{ij}} \quad (9a)$$

$${}^i \tau_{\eta_i} = \sum_{j=1}^{\beta_j} ({}^i p_{\sigma_{ij}} - {}^i p_{\eta_i}) \times (\omega_{\sigma_{ij}} {}^i f_{\sigma_{ij}}) \quad (9b)$$

B. Contact Changes Tracking

At every control step, we can pinpoint the positions of the taxels in contact. When relative sliding occurs during contact, the robot needs to track this sliding to maintain relative stillness with the external contact. This is especially

¹In this work, all weights are uniformly set to 1.

² ${}^i \dot{p}_{\eta_i}$ can be estimated by the time differential of ${}^i p_{\eta_i}$ with the controller step.

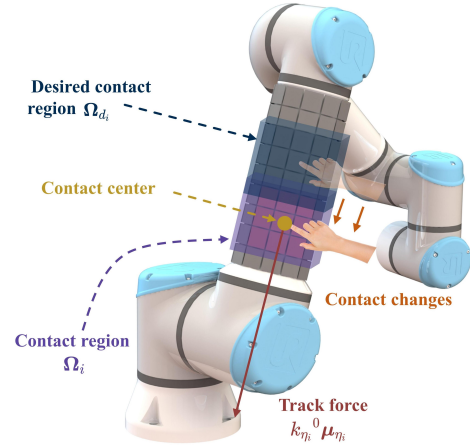


Fig. 4. When the real contact region Ω_i surpasses our desired region Ω_{d_i} , a force $k_{\eta_i} {}^0\mu_{\eta_i}$ will be generated to track the alternation in contact.

meaningful for the electronic skin that can only detect normal forces. An intuitive approach is to describe the contact changes using the movement of the contact center. However, given that poor tactile contact can potentially cause motion in the contact center, we instead represent contact changes using the axis-aligned cubes formed by all the contacting taxels, i.e., the contact region. As illustrated in Fig. 4, if the position of taxels in contact surpasses our desired region, the robot must execute corresponding adjustments to restore the contact within our desired region. This desired region can be derived from past contact regions³.

Considering this, we decide to generate a force ${}^0\mu_{\eta_i} \in \mathbb{R}^3$ acting on the contact center to track contact changes. Upon receiving feedback on the current contact state from tactile sensors, we maintain a cube $\Omega_i \in \{x_i^+, x_i^-, y_i^+, y_i^-, z_i^+, z_i^-\}$ for each link. The edges of this cube represent the maximum and minimum position of all contact taxels, enveloping all currently in-contact taxels on the link with minimal volume. If the contacts on the link surpass the desired region, i.e., when the cube Ω_i extends beyond our desired cube Ω_{d_i} , a track force ${}^0\mu_{\eta_i}$ is generated at the contact center to realign the cube. This track force can be expressed as follows:

$$f_R(x) = \max(x, 0) \quad (10)$$

$${}^0\mu_{\eta_i} = \begin{bmatrix} f_R(x_i^+ - x_{d_i}^+) - f_R(x_{d_i}^- - x_i^-) \\ f_R(y_i^+ - y_{d_i}^+) - f_R(y_{d_i}^- - y_i^-) \\ f_R(z_i^+ - z_{d_i}^+) - f_R(z_{d_i}^- - z_i^-) \end{bmatrix} \quad (11)$$

In this expression, $f_R(x)$ guarantees that track force ${}^0\mu_{\eta_i}$ is activated solely when the desired contact region is surpassed.

C. Contact Point Level Admittance Control

The wrench ${}^0w_{\eta_i} \in \mathbb{R}^6$ exerted on the contact center can be regarded as the sum of the external force ${}^0f_{\eta_i}$, the estimated torque ${}^0\tau_{\eta_i}$, and the track force ${}^0\mu_{\eta_i}$:

$${}^0w_{\eta_i} = \begin{bmatrix} {}^0f_{\eta_i} + k_{\eta_i} {}^0\mu_{\eta_i} \\ {}^0\tau_{\eta_i} \end{bmatrix} \quad (12)$$

³More details can be found in Section V-B.

where the coefficient k_{η_i} governs the magnitude of the track force. The Cartesian admittance control can be described as the behavior of tracking reference trajectory ${}^0x_{r_{\eta_i}} \in \mathbb{R}^6$ under the influence of wrench ${}^0w_{\eta_i}$:

$$\Lambda_i {}^0\ddot{x}_i + D_i {}^0\dot{x}_i + K_i {}^0\tilde{x}_i = {}^0w_{\eta_i} \quad (13)$$

where $\Lambda_i, D_i, K_i \in \mathbb{R}^{6 \times 6}$ are the corresponding desired inertia, damping and stiff matrices. This equation describes the dynamic behavior of the contact center. Besides, ${}^0\tilde{x}_i \in \mathbb{R}^6$ is the deflection that describes the influence of the wrench on the reference trajectory:

$${}^0\tilde{x}_i = {}^0x_{d_{\eta_i}} - {}^0x_{r_{\eta_i}} \quad (14)$$

In this way, the contact center shifts from tracking the initial reference trajectory ${}^0x_{r_{\eta_i}}$ to tracking a new desired trajectory ${}^0x_{d_{\eta_i}} \in \mathbb{R}^6$.

V. CONTROL APPROACH

A. Dynamic Priority for Each Link

For skins without designated interaction tasks, their primary function is to maintain compliance with external contacts. When the skin isn't involved in interaction with the external world, its task shouldn't disrupt ongoing operations. In contrast, when the skin encounters contact with the external environment, it becomes necessary to adapt to these sudden contacts to ensure safety. Hence, establishing priorities for different skins is essential.

Strict priority here is not appropriate. Considering the possible variation of force acting on the skin, the hierarchy of priorities among distinct links may require frequent adjustments. As a result, we provided a simple approach to automatically generate the priority of each link, represented as $\psi_i \in \mathbb{R}$ for each link i :

$$\psi_i = \frac{1 - e^{-b\|{}^0\dot{\tilde{x}}_i\|^2}}{1 + e^{-b\|{}^0\dot{\tilde{x}}_i\|^2}} \quad (15)$$

where ${}^0\dot{\tilde{x}}_i$ is the velocity deflection in (13) and $b \in \mathbb{R}$ is a constant that adjusts the shape of the function. Such a priority function can be seen as a variant of tanh. As the velocity deflection ${}^0\dot{\tilde{x}}_i$ grows due to the external wrench ${}^0w_{\eta_i}$, the weight ψ_i also increases until it approaches the value of 1.

When the weight ψ_i of link i is zero, the robot will not engage in this interaction task of this link. This condition is referred to as "inactivated". In practical applications, a minute positive constant ψ_{thr} is used instead of exactly zero.

B. Desired Trajectory Configuration

As stated in Section V-A, our discussion of interaction tasks is based on two distinct scenarios. In the first scenario, we manually specify the reference trajectory ${}^0x_{r_{\gamma_i}}$, the contact region Ω_i , and the priority ψ_i when we require the contact center to execute certain tasks. On the contrary, in the second scenario, where no specific task has been assigned, all terms above must be generated automatically. We mainly discussed the second scenario here. It's important to note that all tasks

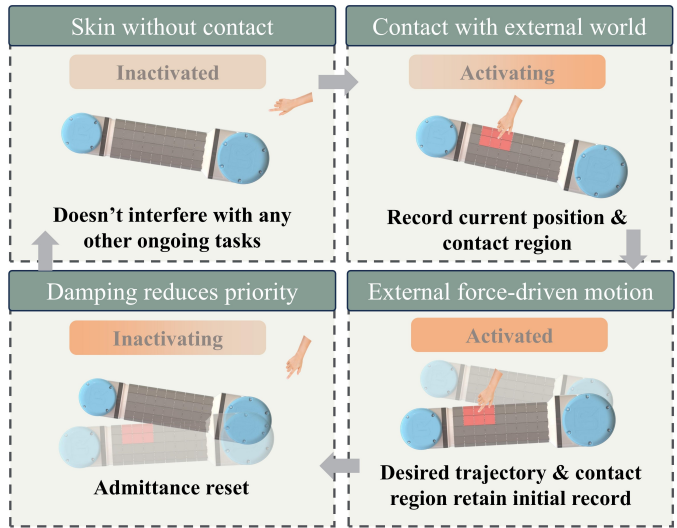


Fig. 5. Illustration of the life-circle of the link i 's interaction. The term "activated" means the weight $\psi_i > \psi_{thr}$, and the term "Activating" means the moment that the weight ψ_i first exceeds the threshold ψ_{thr} .

Algorithm 1: Desired Trajectory Configuration

```

Input:  $\dot{q}, {}^0w_{\eta_i}$ 
Output:  ${}^0x_{d_{\gamma_i}}, \Omega_{d_i}$ 
1 for  $i \leftarrow 0$  to  $\alpha_i$  do
2   update  ${}^0\tilde{x}_i, {}^0\dot{\tilde{x}}_i$ ;
3   update  $\psi_i$ ;
4   if  $\psi_i \geq \psi_{thr}$  then
5      ${}^0x_{d_{\gamma_i}} \leftarrow {}^0x_{t_{\gamma_i}}$ 
6   else
7      ${}^0x_{d_{\gamma_i}} \leftarrow {}^0x_{\gamma_i}$ 
8   end
9   if  $\bar{\psi}_i \geq \psi_{thr}$  and  $\psi_i < \psi_{thr}$  then
10     ${}^0\dot{\tilde{x}}_i, {}^0\tilde{x}_i \leftarrow 0$ 
11   end
12   if  $\bar{\psi}_i \leq \psi_{thr}$  and  $\psi_i > \psi_{thr}$  then
13     ${}^0x_{t_{\gamma_i}} \leftarrow f_{\gamma_i}(\dot{q})$ ;
14     $\Omega_{d_i} \leftarrow \Omega_i$ 
15   end
16    $\bar{\psi}_i \leftarrow \psi_i$ ;
17 end

```

should be defined in the reference frame γ_i due to the varying position ${}^i p_{\eta_i}$ of the contact center.

When link i is not involved in any interaction with the environment, its priority ψ_i is approximately zero and therefore does not interfere with any other ongoing tasks. In this case, we set the reference trajectory ${}^0x_{d_{\gamma_i}}$ of link i to its current actual position ${}^0x_{\gamma_i}$ (in fact, the reference trajectory ${}^0x_{d_{\gamma_i}}$ equals the desired trajectory ${}^0x_{d_{\gamma_i}}$ as ${}^0\tilde{x}_i = 0$). Conversely, when link i starts interacting with the environment, the robot becomes aware of this situation and records the contact position ${}^0x_{\gamma_i}$ and contact region Ω_i at the moment the interaction begins. Throughout the interaction, the robot's reference trajectory ${}^0x_{r_{\gamma_i}}$ is always locked to the position recorded at the onset of the interaction. Once contact is lost,

the link's priority gradually returns to zero due to damping. When it returns to zero, the robot's admittance control is reinitialized, i.e., ${}^0\dot{\tilde{x}}_i, {}^0\tilde{x}_i \leftarrow 0$, and the reference trajectory ${}^0x_{r_{\gamma_i}}$ returns to its current actual position ${}^0x_{\gamma_i}$, waiting for the next moment of activation. This interaction process is illustrated in Figure 5 and Algorithm 1.

For the desired trajectory's orientation part, the reference frame γ_i and contact center η_i are completely identical, and the position part of the desired trajectory in the reference frame γ_i and contact center η_i has the following relationship:

$${}^0p_{d_{\eta_i}} = {}^0p_{d_{\gamma_i}} + {}^0R_{d_i}{}^i p_{\eta_i} \quad (16)$$

$${}^0\dot{p}_{d_{\eta_i}} = {}^0\dot{p}_{d_{\gamma_i}} + {}^0\dot{R}_{d_i}{}^i p_{\eta_i} + {}^0R_{d_i}{}^i \dot{p}_{\eta_i} \quad (17)$$

$${}^0\dot{x}_{d_{\eta_i}} = {}^0\dot{x}_{d_{\gamma_i}} + [{}^0\dot{R}_{d_i}{}^i p_{\eta_i} \quad {}^0R_{d_i}{}^i \dot{p}_{\eta_i} \quad 0]^T \quad (18)$$

Obviously, any interaction behavior on the robot body may lead to deviations from the desired trajectory. To track the desired trajectory, a common choice is task space decomposition velocity control:

$${}^0\dot{x}_{c_{\gamma_i}} = K_p [{}^0p_{d_{\gamma_i}} - {}^0p_{\gamma_i} \quad \log({R_i R_{d_i}})^\vee]^T + {}^0\dot{x}_{d_{\gamma_i}} \quad (19)$$

where $\log({R_i R_{d_i}})^\vee$ is the logarithmic map of the orientation error, represented as a 3-D rotation vector. The control velocity ${}^0\dot{x}_{c_{\eta_i}} \in \mathbb{R}^6$ of the contact center can be obtained by transforming the control velocity of the reference frame:

$$\begin{aligned} {}^0\dot{x}_{c_{\eta_i}} - {}^0\dot{x}_{c_{\gamma_i}} = \\ [K_p({}^0R_{d_i}{}^i p_{\eta_i} - {}^0R_i{}^i p_{\eta_i}) + {}^0\dot{R}_{d_i}{}^i p_{\eta_i} + {}^0R_{d_i}{}^i \dot{p}_{\eta_i} \quad 0]^T \end{aligned} \quad (20)$$

The tracking error can be defined as the error between control velocity ${}^0\dot{x}_{c_{\eta_i}}$ and actual velocity ${}^0\dot{x}_{\eta_i}$:

$${}^0\dot{x}_{e_{\eta_i}} = {}^0\dot{x}_{c_{\eta_i}} - {}^0\dot{x}_{\eta_i} \quad (21)$$

C. QP Formulation

1) *Physical Constraints*: During operation, the robot must respect its own physical constraints. We restrict the robot's joint velocity and confine its joint angles within certain ranges:

$$\begin{aligned} \dot{q}_l \leq \dot{q} \leq \dot{q}_u \\ q_l \leq q + h\dot{q} \leq q_u \end{aligned} \quad (22)$$

where $h \in \mathbb{R}$ is the predictive horizon and q_l, q_u, \dot{q}_l , and $\dot{q}_u \in \mathbb{R}^n$ are lower and upper bound vectors of joint position and velocity.

2) *QP with Constraints*: Our objective is to minimize weighted squared the L2-norm of tracking velocity errors ${}^0\dot{x}_{e_{\eta_i}}$ for all contact centers through optimization of joint velocity \dot{q}^* while adhering multi constraints:

$$\begin{aligned} \dot{q}^* = \arg \min_{\dot{q}} & \sum_{i=1}^{\alpha_i} {}^0\dot{x}_{e_{\eta_i}}^\top \Psi_i {}^0\dot{x}_{e_{\eta_i}} + \varepsilon \dot{q}^\top \dot{q} \\ \text{s.t.} & \dot{q}_l \leq \dot{q}^* \leq \dot{q}_u \\ & \frac{1}{h}(q_l - q) \leq \dot{q}^* \leq \frac{1}{h}(q_u - q) \end{aligned} \quad (23)$$

where $\varepsilon \in \mathbb{R}$ is the regularization term used to reduce ill-conditioning during the QP solving process. In practical ap-

plications, it is set to a small positive value. $\Psi_i = \psi_i \mathbf{I} \in \mathbb{R}^{6 \times 6}$ is the weighting matrix to adjust the priority of tasks for each contact center.

TABLE I
TABLE OF COMPONENTS IN THIS PAPER

n	The DOF of the robot.
\mathbf{q}	$\mathbf{q}^\top = [q_b^\top \quad q_a^\top] \in \mathbb{R}^n$ is the generalized coordinates of the robot.
σ_{ij}	σ_{ij} represents the taxel numbered j on link i .
γ_i	γ_i represents the reference frame of link i , which is selected for convenience.
η_i	η_i represents the contact center of link i .
ψ_i	$\psi_i \in \mathbb{R}$ represents the weight of the contact center η_i .
0R_i	${}^0R_i \in \mathbb{R}^{3 \times 3}$ denotes the rotation of link i , with the assumption that the contact center has the same pose as the link i .
${}^0p_{\eta_i}$	${}^0p_{\eta_i} \in \mathbb{R}^3$ denotes the position of contact center η_i .
Ω_i	$\Omega_i \in \{x_i^+, x_i^-, y_i^+, y_i^-, z_i^+, z_i^-\}$ is the contact region of link i and defined as a cube.
${}^0w_{\eta_i}$	${}^0w_{\eta_i} \in \mathbb{R}^6$ is the wrench of link i as the sum of resultant force ${}^0f_{\eta_i}$, estimated torque ${}^0\tau_{\eta_i}$ and track force ${}^0\mu_{\eta_i}$.
${}^0\tilde{x}_i$	${}^0\tilde{x}_i \in \mathbb{R}^6$ is the deflection of link i .
${}^0x_{d_{\eta_i}}$	${}^0x_{d_{\eta_i}} \in \mathbb{R}^6$ is the desired trajectory of contact center η_i under the influence of contact.
${}^0x_{r_{\eta_i}}$	${}^0x_{r_{\eta_i}} \in \mathbb{R}^6$ is the original reference trajectory of contact center η_i .
${}^0\dot{x}_{c_{\eta_i}}$	${}^0\dot{x}_{c_{\eta_i}} \in \mathbb{R}^6$ is the control velocity of contact center η_i .
${}^0\dot{x}_{e_{\eta_i}}$	${}^0\dot{x}_{e_{\eta_i}} \in \mathbb{R}^6$ is the velocity tracking error of contact center η_i .

VI. EXPERIMENTS

We evaluated our proposed method in several experiments, including basic experiments for specific points and a comprehensive experiment involving a human waltz with a robot⁴. Our experiments were conducted on the hardware platform described in Section III-A, with a control frequency of 100Hz. The data from the tactile sensor has been processed using a moving average filter with a window size of 10. In all experiments, joint velocity commands were computed by OSQP [26], with the parameters ε and h in the QP form (23) manually set to 0.1 and 0.15, respectively. If not otherwise specified, all experiments are conducted with the parameters shown in Table II.

⁴[Online: <https://youtu.be/p-QjIF7wj2o>]

TABLE II
PARAMETERS FOR EXPERIMENTS

\dot{q}_l	\dot{q}_u	q_l	q_u	k_{η_i}	b	K_p	ψ_{thr}
-0.15	0.15	$-\infty$	$+\infty$	200	4	5	10^{-4}

A. Basic experiments

1) **Experiments for contact centering:** The objective of the first experiment is to demonstrate that the contact centers and corresponding wrenches can accurately reflect information about large-area contacts. We mainly considered two scenarios: (i) even contact in single place to test contact forces, (ii) contact on both sides of the same link to test torque estimation. The admittance control matrices of the first experiment is set as $\Lambda_i = 0.5 \cdot I_{6 \times 6}$, $D_i = 40 \cdot I_{6 \times 6}$, $K_i = 0_{6 \times 6}$. The experimental results are illustrated in Fig. 6, and each scenario are numbered over time.

It is worth noting that, to avoid instantaneous large estimated torques, we applied a limit to the estimated torque such that $\tau_{\eta_i}(2) \leq 1.2$. As shown in Fig. 6(B) and Fig. 6(E), the estimated torque quickly reaches the maximum set value, and the joint speed limit is rapidly attained. Another point to note is that at time 2, when the human hand leaves the manipulator, the priority of the contact center does not immediately drop to zero, and the robot continues to move for a short period before stopping. This behavior is expected in admittance control due to the effect of damping.

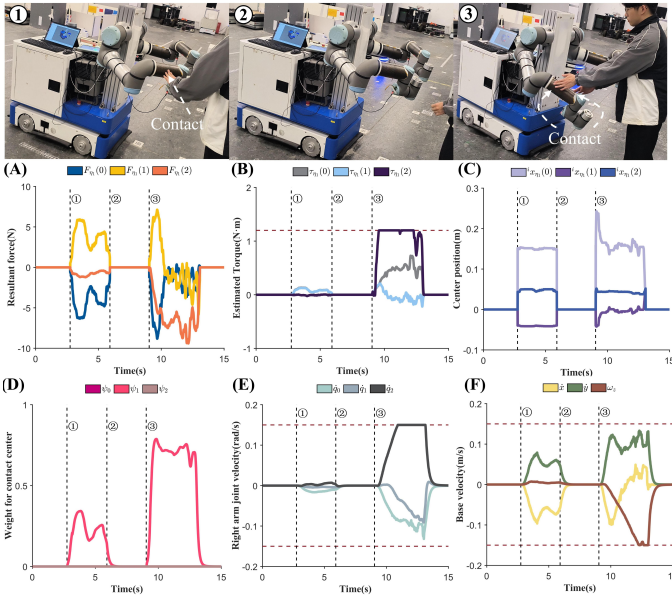


Fig. 6. Experiments for contact centering.

2) **Experiments for contact changes tracking:** The objective of the following experiment is to illustrate that the changes in contact can generate appropriate track force and move the robot in our expected direction. As seen in Fig. 7, The user firstly touches the middle of the contact link, and then slides forward and backward to generate track force. We set a redundancy of 0.01m for the desired contact region

to reduce the sensitivity of the track force. For the sake of easy observation, the operator's contact force is primarily applied in the z-direction, causing slippage in the x and y directions. The admittance control parameters is set as $\Lambda_i = 0.5 \cdot I_{6 \times 6}$, $D_i = diag(40, 40, 500, 40, 40, 40)$, $K_i = 0_{6 \times 6}$. The resulting outcomes are shown in Fig. 7. Initially, the contact slides forward, generating a track force in the direction of the slide. Under the robot's movement, the contact naturally slides back to the initial position, then slides backward, repeating this process. There is a period where the track force is zero, which is due to the current contact region Ω_i being encompassed by the desired contact region $\Omega_{d,i}$. It is worth noting that, unlike other experiments, the robot's initial velocity is not zero when the curve starts. This is because the experimenter has already contact the robot to determine the contact region before sliding occurs.

3) **Experiments for wholebody pHRI:** The purpose of this experiment is to demonstrate that the robot can correctly handle the prioritization of wholebody pHRI tasks in the presence of Cartesian stiffness. The experimenter periodically touches the three links enveloped with the electronic skin on the robot. The admittance parameters for the experiment are set to $\Lambda_i = 0.5 \cdot I_{6 \times 6}$, $D_i = 60 \cdot I_{6 \times 6}$, $K_i = 40 \cdot I_{6 \times 6}$, and the experimental results are shown in Fig. 8. Please note in Fig. 8(D) that as the force stabilizes, the corresponding link's priority gradually decreases to a relatively low value due to the influence of stiffness. When the links are no longer subjected to force, their priority rises again due to the stiffness. In Fig. 8(F) and (G), it can be observed that due to the very small value of ψ_{thr} we set, it has almost no impact on the smoothness of the joint velocity command.

B. Waltz with robot

The experiment of waltzing between a human and a robot is shown in Fig 1. Before the waltz begins, the human adjusts the manipulator's configuration to achieve a comfortable dancing position, which the robot then records as $q_{dance} \in \mathbb{R}^{n_a}$. To accurately represent the dancer's rotation during the dance on the robot's mobile platform instead of the arm, we added manipulator's joint configuration constraints to the kinematic solution: $q_l = q_{dance} - [0.1 \dots 0.1]^\top$, $q_u = q_{dance} + [0.1 \dots 0.1]^\top$. To ensure that the left forearm link remains in contact with the dancer's waist, we applied a constant force of 10N, directed horizontally to the right in the base frame. This is achieved by setting the desired force in the admittance control scheme. Throughout the dance, the priority of the left forearm was kept locked at 1. The admittance control parameters throughout the dance were set as follows: $\Lambda_i = 0.1 \cdot I_{6 \times 6}$, $D_i = 200 \cdot I_{6 \times 6}$, $K_i = 0_{6 \times 6}$. This experiment demonstrated that the dancer could successfully control the robot to follow his dance steps by adjusting the contact force and contact distribution at his waist. More results can be found in the attached videos.

VII. CONCLUSION

In this article, we propose a novel tactile signals processing framework to accomplish complex, large-contact-area whole-body pHRI tasks. For tactile signal processing, we transfer

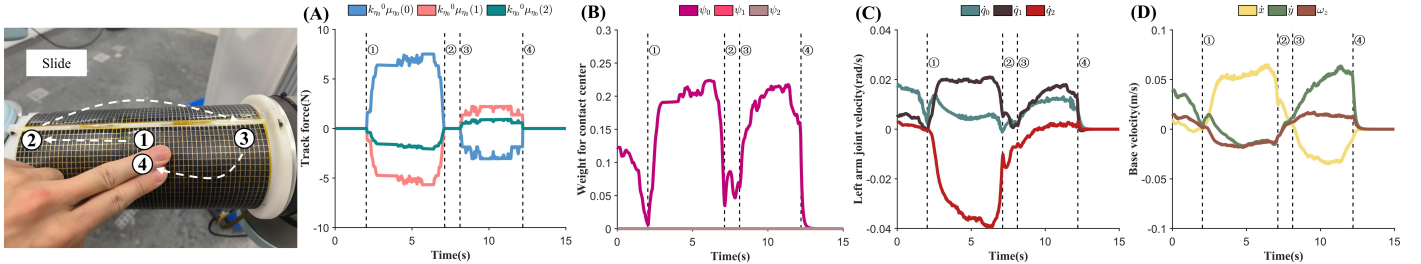


Fig. 7. Experiments for contact changes tracking.

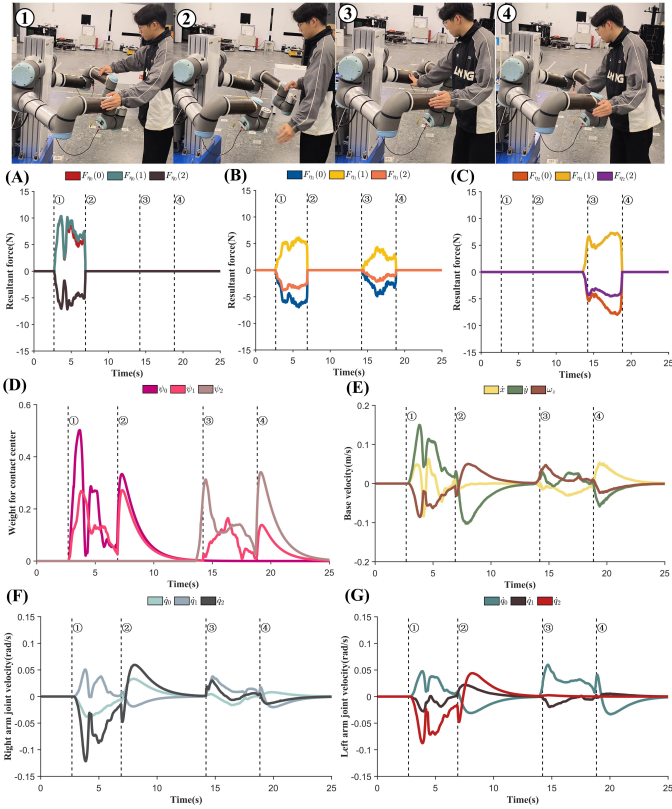


Fig. 8. Experiments for wholebody pHRI.

large-scale contact information to the contact center and estimate the torque and track force to adjust experimental contact. Considering the existence of multiple contact points, we assign a soft priority to each contact center and generate a desired trajectory for them. The proposed method is validated through a series of basic experiments and a comprehensive experiment involving a waltz between the robot and a human. Our future work will focus on employing our framework on humanoid robots and exploring our framework from the perspective of impedance control.

REFERENCES

- [1] K. Park, H. Yuk, M. Yang, J. Cho, H. Lee, and J. Kim, "A biomimetic elastomeric robot skin using electrical impedance and acoustic tomography for tactile sensing," *Science Robotics*, vol. 7, no. 67, p. eabm7187, 2022.
- [2] G. Pang, G. Yang, W. Heng, Z. Ye, X. Huang, H.-Y. Yang, and Z. Pang, "Coboskin: Soft robot skin with variable stiffness for safer human-robot collaboration," *IEEE Transactions on Industrial Electronics*, vol. 68, no. 4, pp. 3303–3314, 2021.
- [3] G. Cheng, E. Dean-Leon, F. Bergner, J. R. G. Olvera, Q. Leboutet, and P. Mittendorfer, "A comprehensive realization of robot skin: Sensors, sensing, control, and applications," *Proceedings of the IEEE*, vol. 107, no. 10, pp. 2034–2051, 2019.
- [4] Z. Li, L. Cheng, and Z. Liu, "Intentional blocking based photoelectric soft pressure sensor with high sensitivity and stability," *Soft Robotics*, vol. 10, no. 1, pp. 205–216, 2023 .
- [5] N. Hogan, "Impedance control: An approach to manipulation," in *1984 American control conference*. IEEE, 1984, pp. 304–313.
- [6] M. Ma and L. Cheng, "A human-robot collaboration controller utilizing confidence for disagreement adjustment," *IEEE Transactions on Robotics*, vol. 40, pp. 2081–2097, 2024.
- [7] T. De Clercq, A. Sianov, and G. Crevecoeur, "A soft barometric tactile sensor to simultaneously localize contact and estimate normal force with validation to detect slip in a robotic gripper," *IEEE Robotics and Automation Letters*, vol. 7, no. 4, pp. 11767–11774, 2022.
- [8] Q. Leboutet, E. Dean-Leon, F. Bergner, and G. Cheng, "Tactile-based whole-body compliance with force propagation for mobile manipulators," *IEEE Transactions on Robotics*, vol. PP, no. 2, pp. 1–13, 2019.
- [9] U. Kim, C.-Y. Maeng, G. Bak, and Y.-J. Kim, "High-stiffness torque sensor with a strain amplification mechanism for cooperative industrial manipulators," *IEEE Transactions on Industrial Electronics*, vol. 69, no. 3, pp. 3131–3141, 2021.
- [10] G. Li, C. Zhang, C. Su, Z. Liu, X. Liang, L. Cheng, and Z.-G. Hou, "Multi-contact intrinsic force sensing method of a flexible finger for hand assistance," *IEEE Transactions on Instrumentation and Measurement*, 2024.
- [11] S. Zhao, W. Liang, K. Wang, L. Ren, Z. Qian, G. Chen, X. Lu, D. Zhao, X. Wang, and L. Ren, "A multiaxial bionic ankle based on series elastic actuation with a parallel spring," *IEEE Transactions on Industrial Electronics*, 2023.
- [12] A. Silva, D. Fonseca, D. M. Neto, M. Babcinschi, and P. Neto, "Integrated design and fabrication of pneumatic

- soft robot actuators in a single casting step,” *Cyborg and Bionic Systems*, vol. 5, p. 0137, 2024.
- [13] H. Sadeghian, L. Villani, M. Keshmiri, and B. Siciliano, “Task-space control of robot manipulators with null-space compliance,” *IEEE Transactions on Robotics*, vol. 30, no. 2, pp. 493–506, 2014.
- [14] T. Kobayashi, E. Dean-Leon, J. R. Guadarrama-Olvera, F. Bergner, and G. Cheng, “Whole-body multicontact haptic human–humanoid interaction based on leader–follower switching: A robot dance of the “box step”,” *Advanced Intelligent Systems*, vol. 4, no. 2, p. 2100038, 2022.
- [15] E. Dean-Leon, F. Bergner, K. Ramirez-Amaro, and G. Cheng, “From multi-modal tactile signals to a compliant control,” in *2016 IEEE-RAS 16th International Conference on Humanoid Robots (Humanoids)*. IEEE, 2016, pp. 892–898.
- [16] M. Leonori, J. M. Gandarias, and A. Ajoudani, “Mocass: a sensitive mobile collaborative robotic assistant exploiting low-cost capacitive tactile cover and whole-body control,” *IEEE Robotics and Automation Letters*, vol. 7, no. 3, pp. 7920–7927, 2022.
- [17] E. Dean-Leon, J. R. Guadarrama-Olvera, F. Bergner, and G. Cheng, “Whole-body active compliance control for humanoid robots with robot skin,” in *2019 International Conference on Robotics and Automation (ICRA)*. IEEE, 2019, pp. 5404–5410.
- [18] S. Armleder, E. Dean-Leon, F. Bergner, and G. Cheng, “Interactive force control based on multimodal robot skin for physical human–robot collaboration,” *Advanced Intelligent Systems*, vol. 4, no. 2, p. 2100047, 2022.
- [19] Q. Leboutet, E. Dean-León, and G. Cheng, “Tactile-based compliance with hierarchical force propagation for omnidirectional mobile manipulators,” in *2016 IEEE-RAS 16th International Conference on Humanoid Robots (Humanoids)*. IEEE, 2016, pp. 926–931.
- [20] J. R. Guadarrama-Olvera, E. Dean-Leon, F. Bergner, and G. Cheng, “Pressure-driven body compliance using robot skin,” *IEEE Robotics and Automation Letters*, vol. 4, no. 4, pp. 4418–4423, 2019.
- [21] A. Dietrich, K. Bussmann, F. Petit, P. Kotyczka, C. Ott, B. Lohmann, and A. Albu-Schäffer, “Whole-body impedance control of wheeled mobile manipulators: Stability analysis and experiments on the humanoid robot rollin’justin,” *Autonomous Robots*, vol. 40, pp. 505–517, 2016.
- [22] E. Magrini, F. Flacco, and A. De Luca, “Estimation of contact forces using a virtual force sensor,” in *2014 IEEE/RSJ International Conference on Intelligent Robots and Systems*. IEEE, 2014, pp. 2126–2133.
- [23] J. Salini, V. Padois, and P. Bidaud, “Synthesis of complex humanoid whole-body behavior: A focus on sequencing and tasks transitions,” in *2011 IEEE international conference on robotics and automation*. IEEE, 2011, pp. 1283–1290.
- [24] M. Karimi and M. Ahmadi, “A reinforcement learning approach in assignment of task priorities in kinematic control of redundant robots,” *IEEE Robotics and Automation Letters*, vol. 7, no. 2, pp. 850–857, 2022.
- [25] P. Mittendorfer, E. Dean, and G. Cheng, “Automatic robot kinematic modeling with a modular artificial skin,” in *2014 IEEE-RAS International Conference on Humanoid Robots*. IEEE, 2014, pp. 749–754.
- [26] B. Stellato, G. Banjac, P. Goulart, A. Bemporad, and S. Boyd, “Osqp: An operator splitting solver for quadratic programs,” *Mathematical Programming Computation*, vol. 12, no. 4, pp. 637–672, 2020.



Yu Sun received his B.S degree from school of aeronautics, Harbin Institute of technology in 2022. He is currently working toward the M.S. degree in the College of Control Science and Engineering, Zhejiang University, Hangzhou, P.R. China. His current research interests include haptics and human-robot interaction.



Cong Xiao received his B.S from school of Artificial Intelligence and Automation, Huazhong University of Science and Technology in 2022. He is currently working toward the M.S. degree in the College of Control Science and Engineering, Zhejiang University, Hangzhou, P.R. China. His current research interests include force control and human-robot collaboration.



Lipeng Chen (Member, IEEE) received the Ph.D. degree from the Robotic Manipulation Lab, University of Leeds, Leeds, UK, in 2019. He was a post-doctoral researcher with the University of Edinburgh, Edinburgh, UK. He is currently a senior research scientist at the Tencent Robotics X Lab, Shenzhen, China. His research interests include autonomous robotic manipulation and physical human-robot collaboration.



Lu Chen received her B.S from college of information and computer, Taiyuan University of Technology in 2016 and received her M.S. from School of Aeronautics and Astronautics, Zhejiang University in 2019. She is currently a Ph.D. candidate in the College of Control Science and Engineering, Zhejiang University, Hangzhou, P.R. China. Her current research interests include force control and physical human-robot collaboration.



Haojian Lu (Member, IEEE) received his PhD in mechanical and electronic engineering with the Department of Mechanical and Biomedical Engineering, City University of Hong Kong, Hong Kong, China. He is currently a Professor in the College of Control Science and Engineering, Zhejiang University, Hangzhou, P.R. China. His latest research interests include soft robotics and physical human-robot interaction.



Yue Wang (Member, IEEE) received his PhD in Control Science and Engineering from College of Control Science and Engineering, Zhejiang University, Hangzhou, P.R. China in 2016. He is currently a Professor in the College of Control Science and Engineering, Zhejiang University, Hangzhou, P.R. China. His latest research interests include human-robot collaboration and robot perception.



Wang-Wei Lee (Member, IEEE) received his Ph.D. degree from the National University of Singapore (NUS) in 2016. He was a Postdoctoral Research Fellow with the Biomedical Institute for Global Health Research and Technology at NUS between 2016 and 2019. He joined Tencent Robotics X in April 2019 as an Advanced Research Scientist in charge of tactile sensor research. His interests include the development of robust tactile sensing technologies applicable to real-world applications. His work ranges from materials engineering, to embedded systems, signal processing and communication to systems integration.



Yu Zheng (Senior Member, IEEE) received the dual B.E. degrees in mechanical engineering and computer science and the Ph.D. degree in mechatronics from Shanghai Jiao Tong University, Shanghai, China, in 2001 and 2007, respectively. He has also received the M.S. and Ph.D. degrees in computer science from the University of North Carolina at Chapel Hill, Chapel Hill, NC, USA, in 2011 and 2014, respectively. In September 2018, he joined Tencent Robotics X, Singapore, where he is currently a Principal Research Scientist and the Team Lead of Control Center. His research interests include multi-contact/multibody robotic systems, robotic grasping and manipulation, legged locomotion, and various algorithms for robotics. Dr. Zheng is an Associate Editor for IEEE Robotics and Automation Letters.



Zhengyou Zhang (Fellow, IEEE) received the B.S. degree in electronic engineering from Zhejiang University, Hangzhou, China, in 1985, the M.S. degree in computer science from the University of Nancy, Nancy, France, in 1987, and the Ph.D. degree in computer science and the Doctorate of Science (Habilitation à diriger des recherches) degree from the University of Paris XI, Paris, France, in 1990 and 1994, respectively. He is currently a Distinguished Scientist and the Director of Tencent Robotics X. Before that, he was a Partner Research Manager with Microsoft Research, Redmond, WA, USA, for 20 years. He received the IEEE Helmholtz Test of Time Award from ICCV 2013 for his article published in 1999 on camera calibration, now known as Zhang's method.



Rong Xiong (Senior Member, IEEE) received her PhD in Control Science and Engineering from the College of Control Science and Engineering, Zhejiang University, Hangzhou, P.R. China in 2009. She is currently a Professor in the College of Control Science and Engineering, Zhejiang University, Hangzhou, P.R. China. Her latest research interests include intelligent mobile manipulation with human-robot collaboration and dynamic motion planning.